From scrap metal to highly efficient electrodes: Harnessing nanotextured surface of swarf for effective utilisation of Pt and Co for hydrogen production

Madasamy Thangamuthu,*[a] Emerson C. Kohlrausch,[a] Ming Li,[b] Alistair Speidel,[b] Adam T. Clare,[b] Richard Plummer,[a] Paul Geary,[c] James W. Murray,[b] Andrei N. Khlobystov*[a] and Jesum Alves Fernandes*[a]

[a] School of Chemistry, University of Nottingham, University Park, Nottingham NG7 2RD, United Kingdom

[b] Faculty of Engineering, University of Nottingham, University Park, Nottingham NG7 2RD, United Kingdom

[c] Aqsorption, 15A Great Northern Way, Netherfield, Nottingham NG4 2HD, United Kingdom

E-mail: madasamy.thangamuthu1@nottingham.ac.uk, andrei.khlobystov@nottignham.ac.uk, jesum.alvesfernandes@nottingham.ac.uk

Supporting information

Table S1: Nominal composition of 304L, Ti-6Al-4V, Inconel 625 and 718

304L steel	Fe Bal	Cr 17.5	Ni 8.0-10.5	Mn 2.0	Si 1.0	P 0.045	C 0.03	S 0.015
Ti-6Al-4V	Ti 87.6-91	Al 5.5-6.75	V 3.5-4.5	Fe < 0.4	O < 0.2	C < 0.08	N < 0.05	H <0.015
Inconel 625	Ni Bal	Cr 22.3	Mo 9	Fe 4.5	Nb 3.5	Ti 0.2	Al 0.19	Si 0.16
Inconel 718	Ni Bal	Cr 18.4	Mo 3	Fe 18	Nb 5.0	Ti 0.9	Al 0.6	Si 0.08

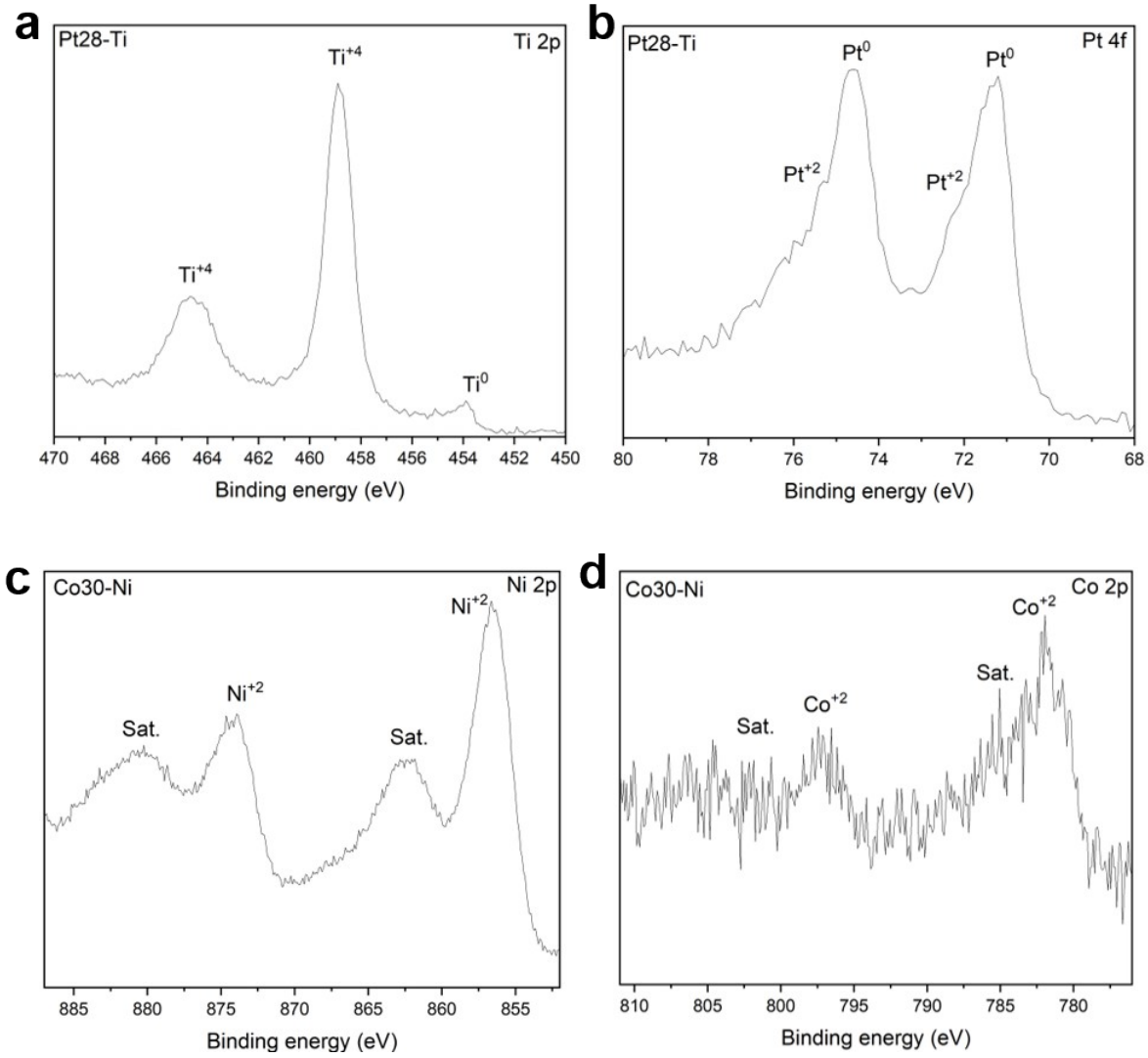

Figure S1. XPS spectra of a) Ti 2p, b) Pt 4f, c) Ni 2p, and d) Co 2p of the swarf electrodes.

Table S2: Details of HER and OER electrocatalyst loaded on the swarf electrodes using atom sputtering

Swarf electrode	**Electrocatalyst**	**Deposition time (s)**	**Amount of electrocatalyst loading (mg cm^{-2})**
Ti	Pt	45	0.013
Ti	Pt	90	0.0275
Ti	Pt	180	0.060
Inconel 625	Co	45	0.0149
Inconel 625	Co	90	0.030
Inconel 625	Co	180	0.068
Inconel 625	Ru	45	0.016
Inconel 625	Ru	90	0.025
Inconel 625	Ru	180	0.0490

Table S3. Comparison of EIS parameters of the HER and OER electrodes

Electrodes	**R_S (Ω)**	**R_{SC} (Ω)**	**R_{cat} (Ω)**	**R_H (Ω)**	**R_p (Ω)**	**C_{SC} (μF cm^{-2})**	**C_{cat} (μF cm^{-2})**	**C_H (μF cm^{-2})**
HER								
Ti	2.5	1365	-	11.1	1376.1	197	-	268
Pt13-Ti	2.7	96.9	11.3	1.06	109.26	204	289	119
Pt28-Ti	2.75	8.73	3.5	0.47	12.7	382	366	84.6
Pt60-Ti	2.6	20.6	3.97	0.6	25.17	282	220	91.2
SST	3.0	205	-	6.6	211.6	268	-	256
Pt13-SST	3.2	144	17.6	1.34	162.94	301	306	149
Pt28-SST	2.6	65.5	11.9	1.28	78.97	507	355	118
Pt60-SST	2.6	150	21.0	1.57	172.57	404	395	214
Pt28-Ni	2.6	12.5	1.49	0.48	14.5	844	815	295
OER								
Ni	1.88	9.49	-	0.37	11.68	2806	-	971
Co15-Ni	1.9	3.5	0.21	0.27	3.98	4679	7642	277
Co30-Ni	1.8	2.27	0.2	0.05	2.52	12340	21160	4160
Co68-Ni	1.9	3.05	0.45	0.1	3.6	5350	8630	3992

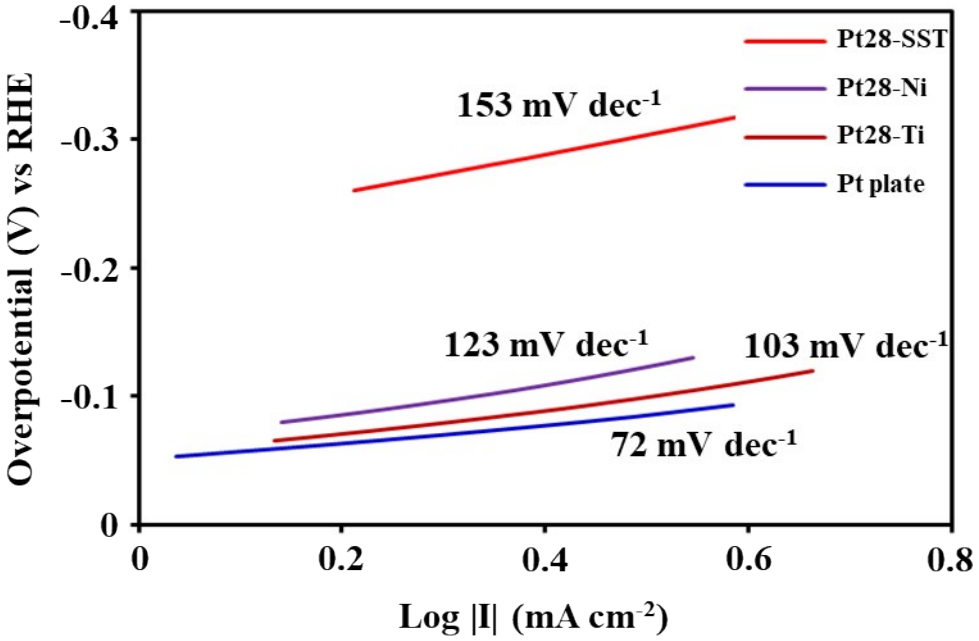

Figure S2. Tafel plots for Pt plate, Pt28-Ti, Pt28-Ni, and Pt28-SST.

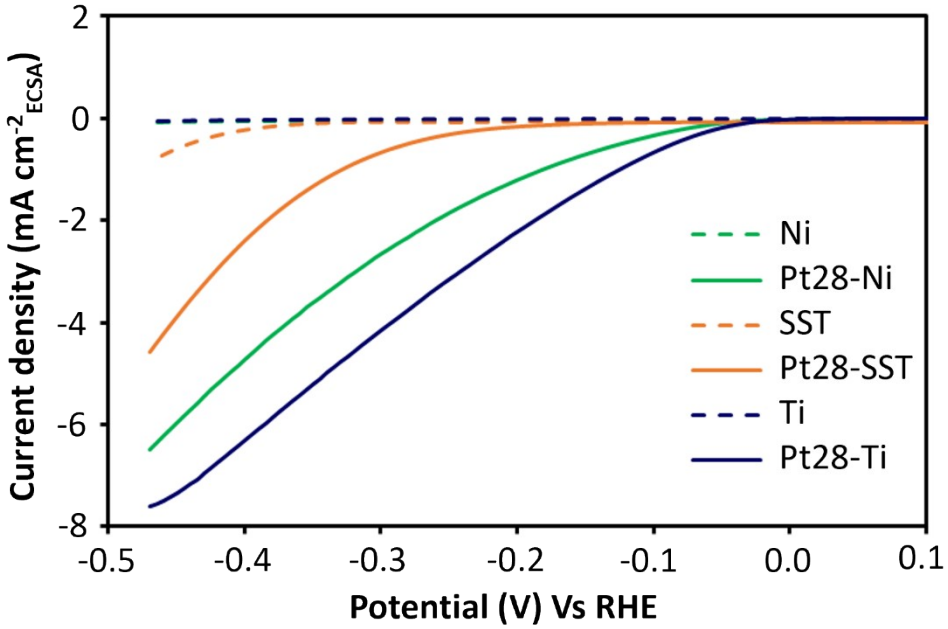

Figure S3. The hydrogen evolution activities of the Ni, Pt28-Ni, SST, Pt28-SST, Ti, and Pt28-Ti measured in 1 M KOH solution at scan rate 10 mV s^{-1} vs. Hg/HgO. The current values are normalised to the ECSA values of the corresponding electrodes.

The HER activity is in the order of Pt28-Ti > Pt28-Ni > Pt28-SST, which is similar to the activity obtained normalised to the electrode's geometric area (Figure 1a), showing that the intrinsic activity of the electrodes do not alter.

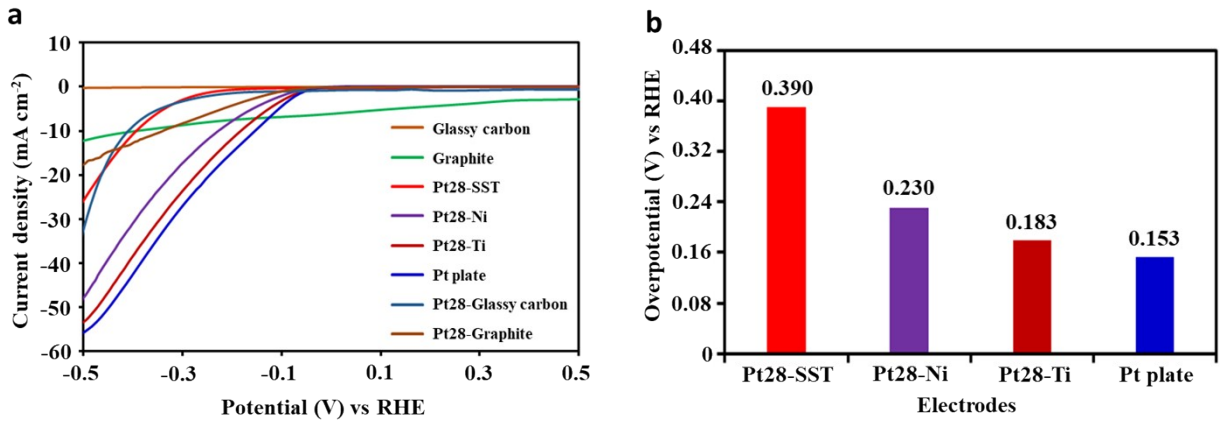

Figure S4. a) Comparison of HER activities of Pt28-Ti, Pt28-Ni, Pt28-SST, commercial Pt plate, glassy carbon, Pt28-glassy carbon, graphite, and Pt28-graphite electrodes, b) overpotential derived from LSV polarisation curve at 10 $mAcm^{-2}$ for Pt28-Ti, Pt28-Ni, Pt28-SST, and commercial Pt plate (note: the current density value of the glassy carbon and graphite rod electrodes not included).

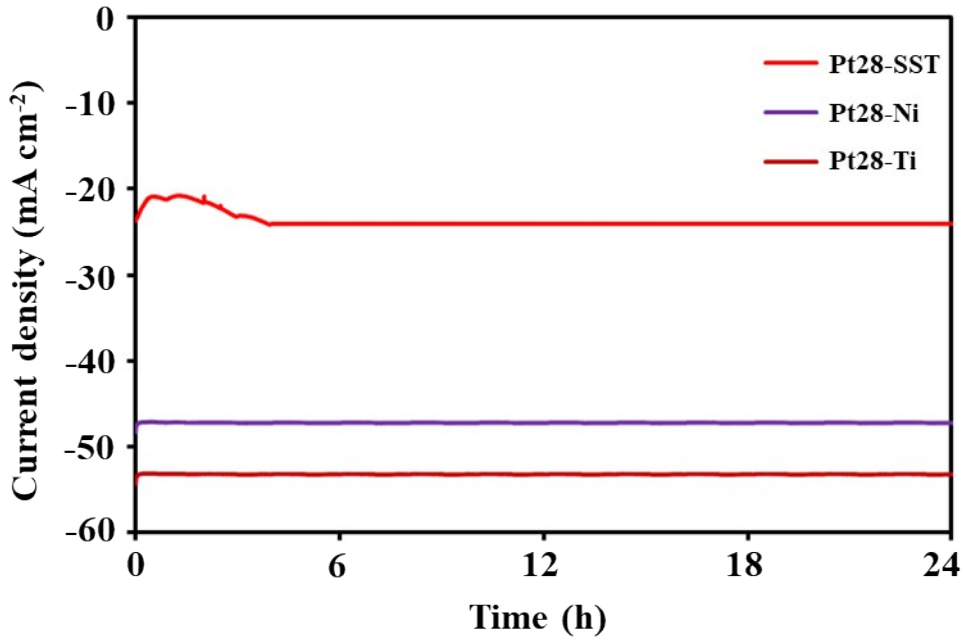

Figure S5. Long-term stability test of Pt28-Ti, Pt28-Ni, and Pt28-SST in 1 M KOH at a constant potential of -0.5 V vs RHE.

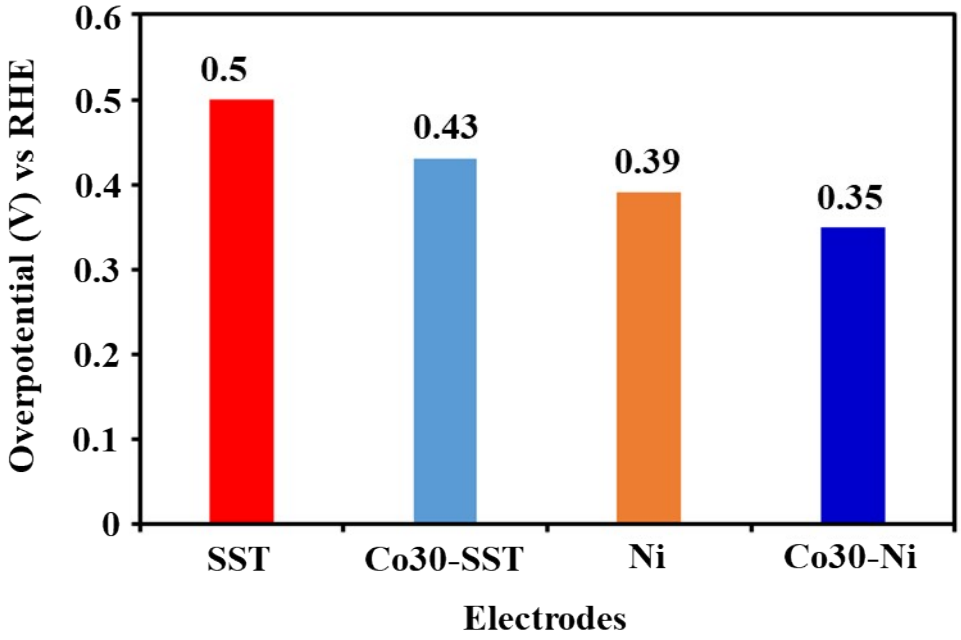

Figure S6. Overpotential derived from LSV polarisation curve at 10 $mAcm^{-2}$ for SST, Co30-SST, Ni, and Co30-Ni (note: the overpotential value for Ti and Co30-Ti were not included as they are not able to produce 10 mA cm^{-2}).

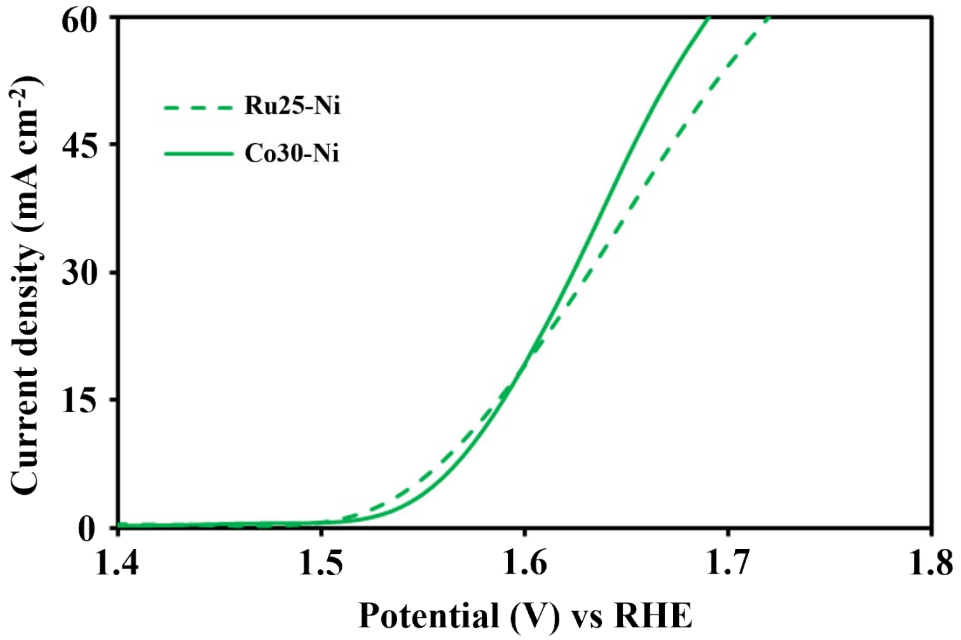

Figure S7. OER performance of the Ru25-Ni, Co30-Ni electrodes in 1 M KOH (5.6%) at scan rate 10 mV s^{-1} vs. Hg/HgO.

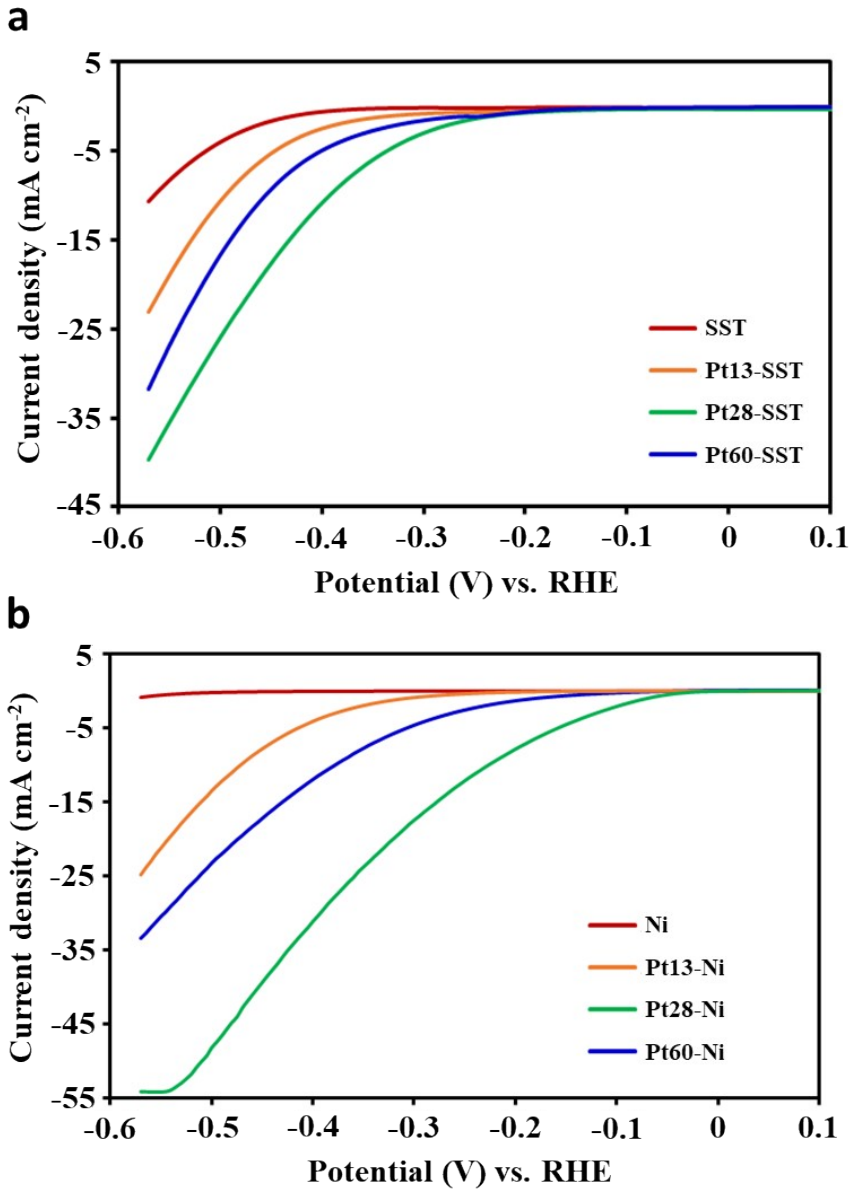

Figure S8. HER performance of a) bare SST, Pt13-SST, Pt28-SST, Pt60-SST, b) bare Ni, Pt13-Ni, Pt28-Ni, Pt60-Ni in 1 M KOH at scan rate 10 mV s^{-1} vs. Hg/HgO.

Electrochemical active surface area calculation:

The electrochemically active surface area (ECSA) of the electrodes was calculated based on the double-layer capacitance at the electrode-electrolyte interface using equation 9.

$$ECSA = \frac{C_{DL}}{C_s} \quad (9)$$

To determine the C_{dl}, we measured the non-faradaic capacitive current associated with double-layer charging using cyclic voltammetry. This was performed at various scan rates ranging from 20 to 100 mV s^{-1} within the potential range of 0 to 0.2 V vs. Hg/HgO. The CVs of the Ti swarf electrode series including Ti, Pt13-Ti, Pt28-Ti, and Pt60-Ti show the increased capacitive current while increasing the scan rates (**Figure S9**). The double-layer capacitance values were determined by analysing the current-scan rate plot (**Figure 2e and f**). To compute the ECSA of the electrodes, we divided the C_{dl} by the specific capacitance of the planar surface per unit area under identical electrolyte conditions. We estimated the C_S to be 40 µF cm^{-2} in experimental conditions (typical C_S values for alkaline solutions range from 22 to 130 µF cm^{-2}).[1] Notably, we did not consider other possible contributions, such as pseudo capacitance due to ion adsorption and chemical capacitance due to electron trap states, in the measured C_{dl}.

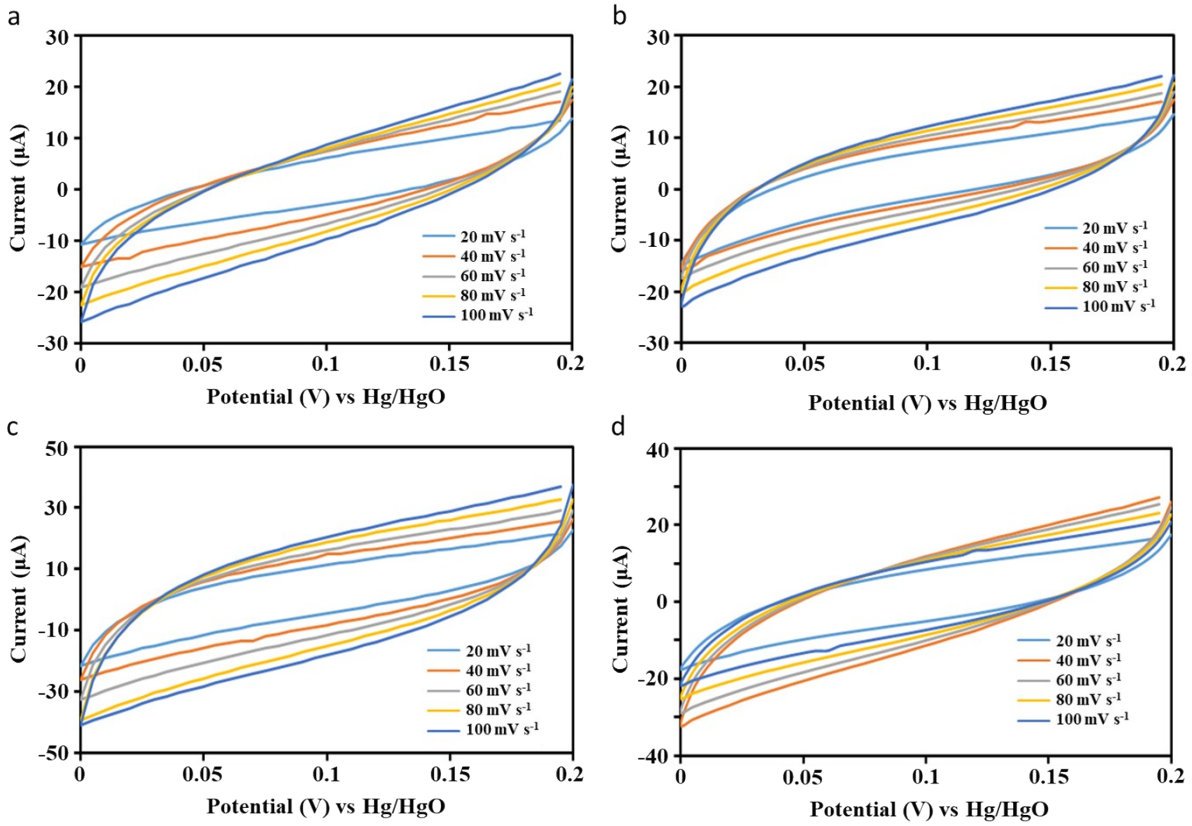

Figure S9. Cyclic voltammograms of a) Ti, b) Pt13-Ti, c) Pt28-Ti, and d) Pt60-Ti measured in 1 M KOH solution at the scan rate of 20, 40, 60, 80, and 100 mV s^{-1}. All current is assumed due to the double-layer charging. The current difference between forward and backward sweep at 0.1 V was used to plot a scan rate vs. current graph, which gives the slope value corresponding to the double-layer capacitance.

Table S4. The double-layer capacitance of the HER and OER electrodes and their ECSA

Electrodes	Double layer capacitance C_{dl} (µF)	Electrochemical active surface area (ECSA = $\frac{C_{DL}}{C_S}$) cm²
HER		
Ti	34.80	0.87
Ni	110.0	2.75
SST	113.50	2.84
Pt13-Ti	46.50	1.16
Pt28-Ti	282.70	7.07
Pt60-Ti	92.30	2.31
Pt28-Ni	267.0	6.6
Pt28-SST	182.5	4.56
OER		
Co15-Ni	119.00	2.97
Co30-Ni	170.63	4.34
Co68-Ni	127.00	3.17
Co30-SST	122.60	3.06
Co30-Ti	88.56	2.21

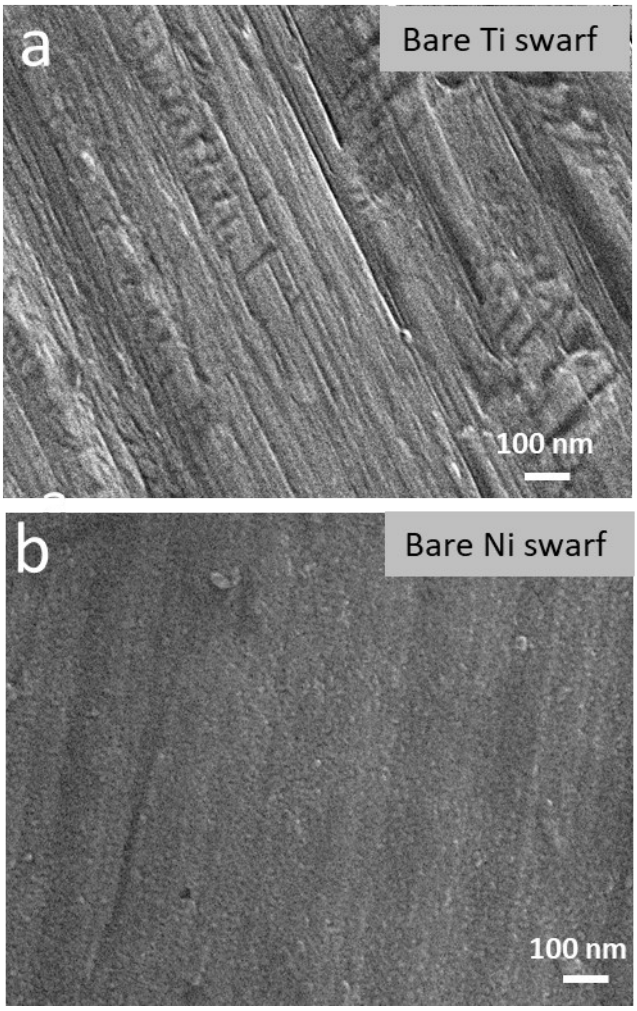

Figure S10: SEM images of the a) bare Ti, and b) bare Ni swarf electrodes.

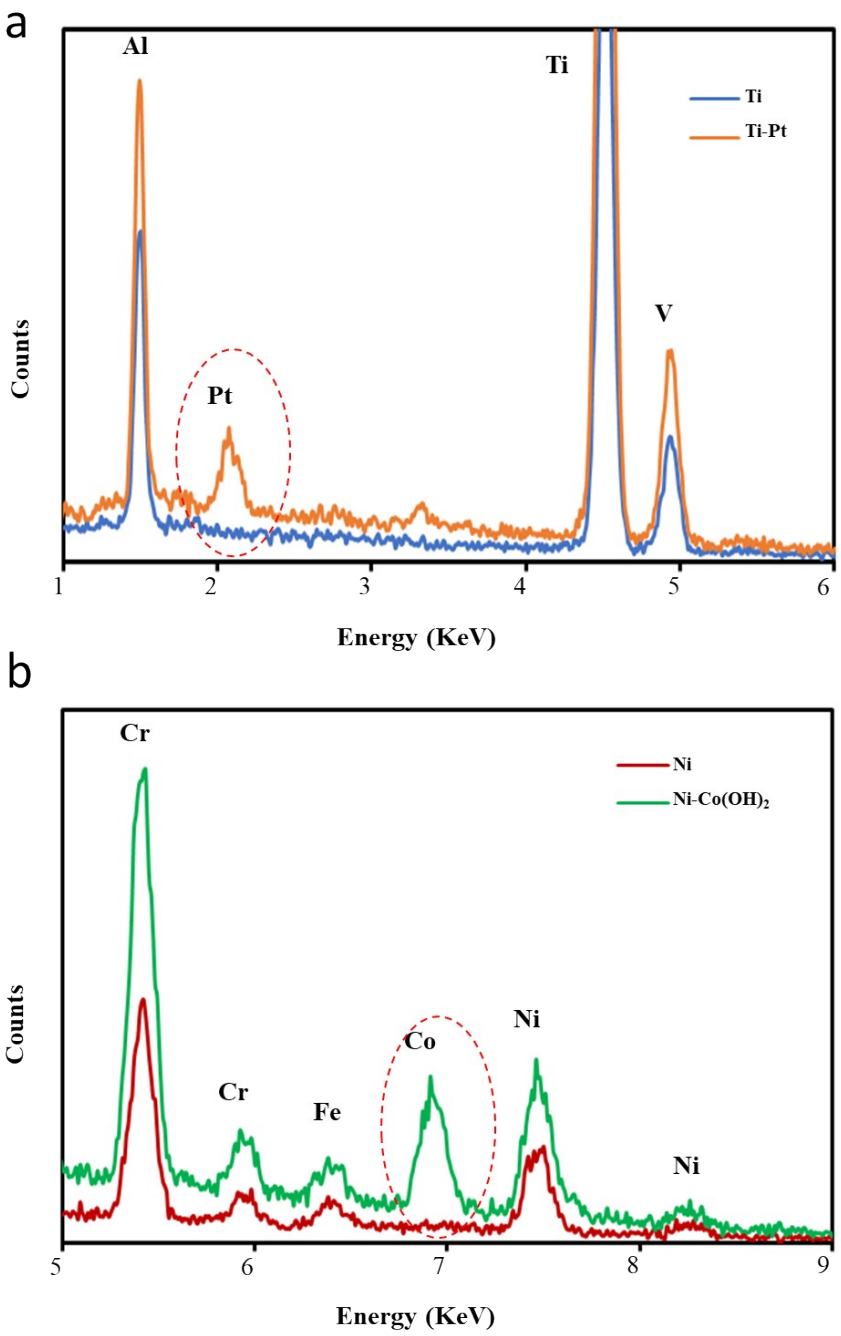

Figure S11: EDX spectra of o) Pt on Ti (Al and V are part of the Ti alloy) and p) $Co(OH)_2$ on Ni (Cr and Fe are part of the Ni alloy).

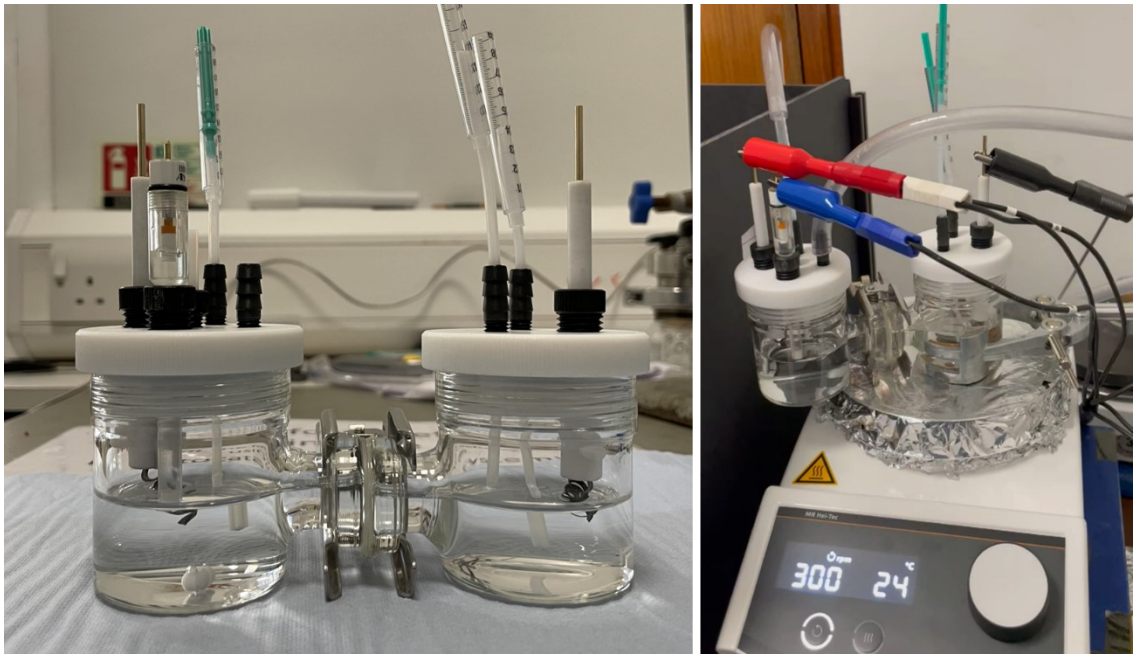

Figure S12. Photograph of the full-cell comprised of Ti-Pt (medium) and Ni-$Co(OH)_2$ electrodes and are separated by an anion exchange membrane.

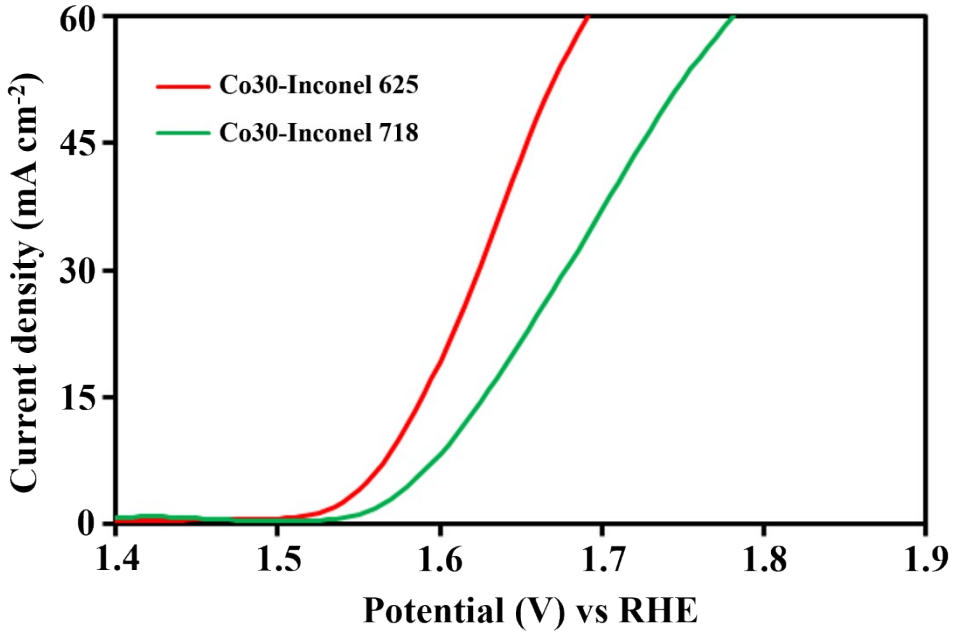

Figure S13: Comparison of OER activity of the Inconel 625 (balance%Ni, 22.3%Cr, 9%Mo, 4.5%Fe, 3.5%Nb, 0.2%Ti, 0.19%Al, and 0.16%Si) and Inconel 718 (balance%Ni, 18.4%Cr, 3%Mo, 18%Fe, 5%Nb, 0.9%Ti, 0.6%Al, 0.08%Si) commercial alloys swarf after depositing 30 µg cm^{-2} of cobalt measured in 1 M KOH (5.6%) at scan rate 10 mV s^{-1} vs. Hg/HgO.

Figure S14: A photograph of a tailor-made sample holder for Pt atoms deposition on the swarf surface.

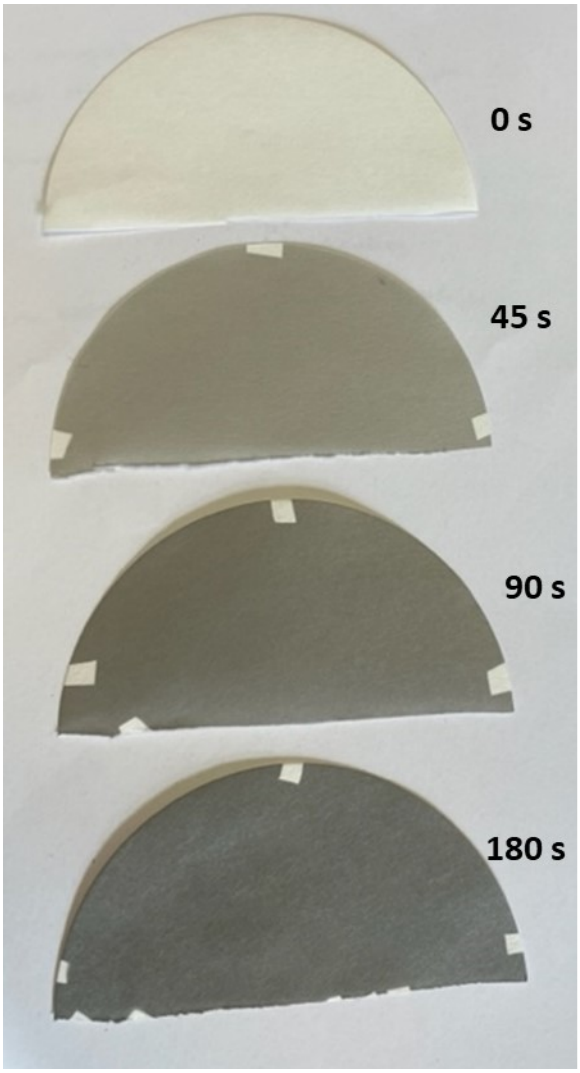

Figure S15: A photograph of the Pt atoms deposited on the filter papers with three weight loadings.

Table S5: Comparison of the present HER half-cell performance with earlier reports under alkaline (1 M KOH) conditions

Electrodes	Over potential at 10 mA cm^{-2}	Faradaic Efficiency (%)	Tafel slope (mV dec^{-1})	Electrocatalyst loading	Reference
SST-NiP	0.268 V	N/A	70.5	Electrodeposition forms large dendrite structure	[2]
NPSSF-Pt	0.07 V	N/A	76.8	In-situ reduction forms ~100 nm particles	[3]
SST- NiFeP	0.210 V	N/A	119	Electrodeposition of Ni, Fe and P (60, 35 and 5%wt)	[4]
Ti-NiCo	0.125	N/A	47	Electrodeposition of NiCo thin film	[5]
*Cu foam-PtNC	0.033	N/A	61	In-situ wet chemistry growth of ~30 nm pt nanocrystals with 0.3 mg cm^{-2} loading	[6]
*CP/Pt_8Co	0.047	N/A	50	Wet chemistry method synthesis of PtCo and 0.045 mg cm^{-2} loaded on carbon paper	[7]
*CP/C-Pt	0.187	N/A	124	Commercial Pt/C ink drop-casted on carbon paper	[7]
3D carbon foam-PtNPs	0.105	N/A	0.105	Electrodeposition of forms ~50 nm PtNPs and 0.06 mg cm^{-2} loaded on carbon foam	[8]
Ni foam/NiO-PtSA	0.050	N/A	25	Electrodeposition	[9]
Ni foam/PtNPs	0.200	N/A	N/A	Sputtering of PtNPs forms film and 38wt% of Pt loaded on Ni foam.	[10]
Swarf Pt-Ti	0.183 V	100%	103	Atomic deposition of Pt directly on Ti swarf with 0.028 mg cm^{-2} loading	This work

*Previous reports utilized Ag/AgCl as a reference electrode in a 1 M KOH electrolyte. However, the corrosive nature of KOH adversely affects the microporous frit at the tip of the reference electrode, compromising the electrocatalytic performance of the materials. Consequently, the reliability of these results is questionable. To address this issue, we strongly recommend employing Hg/HgO reference electrode for enhanced accuracy and stability in future investigations.

Table S6: Comparison of the present OER half-cell performance with earlier reports under alkaline (1 M KOH) condition

Electrodes	**Over potential at 10 mA cm^{-2}**	**Faradaic efficiency (%)**	**Tafel slope (mV dec^{-1})**	**Electrocatalyst loading**	**Reference**
*SST	0.37 V	96	30	N/A	[11]
Ti/NiCo	0.331 V	N/A	60	Electrodeposition forms NiCo film on titanium foil	[5]
*Ti/TiOx-BCN	0.400 V	100	N/A	Plasma CVD deposition forms TiOx-BCN film on titanium foil	[12]
SST-NiP	0.238 V	N/A	41.24	Electrodeposition forms large dendrite structure of NiP	[2]
SST-NiFeP	0.305	N/A	88	Electrodeposition of Ni, Fe and P on SST substrate with 60, 35 and 5%wt	[4]
SST- $Ni_xFe_yO_z$	0.22	100	49	Electro-oxidation of AISI 304 steel	[13]
*SST-Co_3O_4	0.298	N/A	105	Microwave synthesis forms Co_3O_4 with 1.17 mg cm^{-2} weight loading	[14]
*C/$Co(OH)_2$-$Mg(OH)_2$	0.443	N/A	N/A	Polyol method synthesis $Co(OH)_2$ and $Mg(OH)_2$ and 21.7% Co and 11.5% Mg	[15]
GC-m-Co-OH	0.32 V	N/A	N/A	Wet chemistry synthesis forms m-Co-OH thin film on glassy carbon	[16]
GC/BN-graphene/ CoOx NP	0.295	97.4	57	Wet chemistry	[17]
GC/$Co(OH)_2$/SWNTs	0.235	N/A	60	Wet chemistry Thin film	[18]
Co-Ni	0.35 V	100	54.6	Atom deposition 0.03 mg cm^{-2} or 0.085wt%	This work

*Previous reports utilized Ag/AgCl as a reference electrode in a 1 M KOH electrolyte. However, the corrosive nature of KOH adversely affects the microporous frit at the tip of the reference electrode, compromising the electrocatalytic performance of the materials. Consequently, the reliability of these results is questionable. To address this issue, we strongly recommend employing Hg/HgO reference electrode for enhanced accuracy and stability in future investigations.

References

[1] C. C. L. McCrory, S. Jung, J. C. Peters, T. F. Jaramillo, *J Am Chem Soc* **2013**, *135*, 16977.

[2] A. Z. Alhakemy, A. B. Ahmed Amine Nassr, A. E.-H. Kashyout, Z. Wen, *Sustain Energy Fuels* **2022**, *6*, 1382.

[3] Y. Tan, Y. Wei, K. Liang, L. Wang, S. Zhang, *Int J Hydrogen Energy* **2021**, *46*, 26340.

[4] S. Cartagena, F. E. Bedoya-Lora, J. A. Calderón, *J Electrochem Soc* **2022**, *169*, 044501.

[5] P. Ganesan, A. Sivanantham, S. Shanmugam, *ACS Appl Mater Interfaces* **2017**, *9*, 12416.

[6] Y. Tan, R. Xie, S. Zhao, X. Lu, L. Liu, F. Zhao, C. Li, H. Jiang, G. Chai, D. J. L. Brett, P. R. Shearing, G. He, I. P. Parkin, *Adv Funct Mater* **2021**, *31*, 2105579.

[7] J. Hu, C. Fang, X. Jiang, D. Zhang, Z. Cui, *Inorg Chem Front* **2020**, *7*, 4377.

[8] A. H. Ghanim, J. G. Koonce, B. Hasa, A. M. Rassoolkhani, W. Cheng, D. W. Peate, J. Lee, S. Mubeen, *Front Chem* **2018**, *6*.

[9] K. L. Zhou, Z. Wang, C. B. Han, X. Ke, C. Wang, Y. Jin, Q. Zhang, J. Liu, H. Wang, H. Yan, *Nat Commun* **2021**, *12*, 3783.

[10] R. G. Milazzo, S. M. S. Privitera, D. D'Angelo, S. Scalese, S. Di Franco, F. Maita, S. Lombardo, *Int J Hydrogen Energy* **2018**, *43*, 7903.

[11] F. Yu, F. Li, L. Sun, *Int J Hydrogen Energy* **2016**, *41*, 5230.

[12] N. Jiménez-Arévalo, F. Leardini, I. J. Ferrer, J. R. Ares, C. Sánchez, M. M. Saad Abdelnabi, M. G. Betti, C. Mariani, *ACS Appl Energy Mater* **2020**, *3*, 1922.

[13] H. Schäfer, S. Sadaf, L. Walder, K. Kuepper, S. Dinklage, J. Wollschläger, L. Schneider, M. Steinhart, J. Hardege, D. Daum, *Energy Environ Sci* **2015**, *8*, 2685.

[14] A. R. Jadhav, J. M. C. Puguan, H. Kim, *ACS Sustain Chem Eng* **2017**, *5*, 11069.

[15] I. Hwang, I. Jang, G. Lee, Y. Tak, *Int J Electrochem Sci* **2016**, *11*, 6204.

[16] M. A. Ghanem, A. M. Al-Mayouf, P. Arunachalam, T. Abiti, *Electrochim Acta* **2016**, *207*, 177.

[17] Y. Tong, P. Chen, T. Zhou, K. Xu, W. Chu, C. Wu, Y. Xie, *Angewandte Chemie International Edition* **2017**, *56*, 7121.

[18] D. McAteer, I. J. Godwin, Z. Ling, A. Harvey, L. He, C. S. Boland, V. Vega-Mayoral, B. Szydłowska, A. A. Rovetta, C. Backes, J. B. Boland, X. Chen, M. E. G. Lyons, J. N. Coleman, *Adv Energy Mater* **2018**, *8*, 1702965.